International Journal of Automotive Technology, Vol. 8, No. 5, pp. 583–591 (2007)

1229-9138/2007/036-06

H_∞ LATERAL CONTROL OF AN AUTONOMOUS VEHICLE USING THE RTK-DGPS

J. H. RYU[1)*], C. S. KIM[1)], S. H. LEE[2)] and M. H. LEE[3)]

[1)]Department of Mechanical and Intelligent Systems Engineering, Pusan National University, Busan 609-735, Korea
[2)]Interdisciplinary Program in Mechatronics, Pusan National University, Busan 609-735, Korea
[3)]School of Mechanical Engineering, Pusan National University, Busan 609-735, Korea

(Received 16 June 2006; Revised 15 July 2007)

ABSTRACT–This paper describes the development of the H_∞ lateral control system for an autonomous ground vehicle operating a limited area using the RTK-DGPS (Real Time Kinematic-Differential Global Positioning System). Before engaging in autonomous driving, map data are acquired by the RTK-DGPS and used to construct a reference trajectory. The navigation system contains the map data and computes the reference yaw angle of the vehicle using two consecutive position values. The yaw angle of the vehicle is controlled by the H_∞ controller. A prototype of the autonomous vehicle by the navigation method has been developed, and the performance of the vehicle has been evaluated by experiment. The experimental results show that the H_∞ controller and the RTK-DGPS based navigation system can sufficiently track the map at low speed. We expect that this navigation system can be made more accurate by incorporating additional sensors.

KEY WORDS : Autonomous vehicle, Navigation algorithm, H_∞ control, Lateral control, RTK-DGPS and Electric compass

1. INTRODUCTION

Research centered on ITS (Intelligent Transportation System), PATH (Partners for Advanced Transit and Highways) and AHS (Automated Highway System) has led to the development of the autonomous vehicle (Broggi *et al.*, 1999). Although magnetoresistive (MR) and vision sensors play an enabling part in autonomous vehicle operation, they are not sufficient to permit operation under all conditions (Huei *et al.*, 1992). For example, MR sensors require marked magnet points on the road and are susceptible to stochastic error. A disadvantage of vision sensors is that they are sensitive to weather conditions and light (Lee *et al.*, 2002; Lee *et al.*, 2006). Vehicle navigation by using an absolute coordinate system has now progressed to a practical level (Miguel *et al.*, 2001). In this paper, we analyze the case of an autonomous vehicle navigating by an absolute coordinate system with an RTK-DGPS (Real Time Kinematic-Differential Global Positioning System).

GPS is an all-weather, worldwide, continuous coverage, satellite-based radio navigation system (Jay, F. and Matthew, 1998). GPS receivers calculate position by measuring time delays; they decode messages from in-view satellites to calculate position and time bias. Although the measurement of the satellite-to-receiver range in the GPS system is subject to several types of error, differential GPS has been used to improve the accuracy of GPS.

DGPS adds a land-based reference receiver located at an accurately surveyed site. Since the reference station knows where the satellites are located in space at any given moment, as well as its own exact location, the station can compute the theoretical distance and signal travel times between itself and each satellite. When these theoretical measurements are compared to actual satellite transmissions, any differences represent the error in the satellite's signal. All DGPS reference stations have transmitters to forward the error factors to DGPS receivers by radio or other methods, and the GPS receiver uses this data to correct its own measurements and calculations. This differential correction technique applies to GPS receivers performing code-phase navigation.

When a receiver navigates in carrier-phase mode, it is measuring a different GPS observable, namely the GPS carrier wave. To obtain high accuracy with carrier-phase measurements, it is necessary to compute the number of GPS wavelengths between the roving GPS receiver's antenna and the satellites using information (i.e., carrier-phase measurements) from a base receiver. This techni-

*Corresponding author. e-mail: neo@pusan.ac.kr

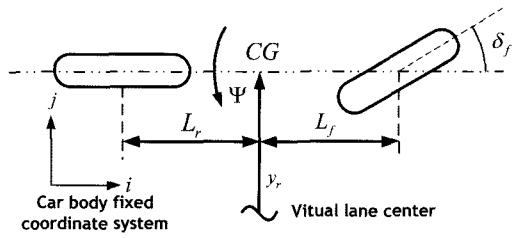

Figure 1. Linear 2 DOF vehicle mode.

que, called RTK-DGPS, yields accuracy to the cm-level in dynamic environments. The method is thus useful for making a digital road map and computing vectors for navigation. The use of RTK-DGPS in autonomous vehicles has been researched through integration with image processing (Naranjo *et al.*, 2005). This approach is aided by INS (Tan *et al.*, 2003). Fuzzy logic controllers have been applied to autonomous vehicles to accommodate variation of vehicle parameters (Ryu *et al.*, 2004; Naranjo *et al.*, 2005). These are designed and tuned according to a verbal description of driver experience.

Usually, the reference detection system for an unmanned vehicle uses the look-ahead system and the look-down system (Chen *et al.*, 1998). The look-ahead system, in the form of a vision system, computes the lateral position of a vehicle from upcoming-lane information. The look-down system computes the lateral position in a different way, as the sensor adhering to the bump detects the guideline in the center of the road. In this paper, lateral control of the autonomous vehicle was achieved by using a reference yaw angle that was calculated by using the current position and the map data. In addition, the attitude of the vehicle was sensed in real time by a digital compass. The map data was constructed by the RTK-DGPS system before commencing unmanned driving. In this approach, the navigation system located a proper target point in the map data, and the next point was found by considering the velocity of the vehicle. Finally, the property of the navigation system was evaluated by using a prototype unmanned vehicle.

The H_∞ control system, which uses the feedback of the yaw angle error, was used to design a robust lateral control against modeling uncertainty (Shladover, 1991). The performance of this algorithm is compared to that of the PID controller.

The remainder of this paper is organized as follows. First, section 2 provides the algorithm for H_∞ lateral control of vehicle yaw. Section 3 suggests an RTK-DGPS-based navigation algorithm. The algorithm for navigation and conventional lateral control is discussed in section 4. Finally, section 5 summarizes the results presented in this paper and suggests future work.

2. LATERAL CONTROL BY LOOK-DOWN SENSING

2.1. Lateral Vehicle Models

This section considers a classic linearized bicycle model with two degrees of freedom for the lateral and yaw dynamics of a vehicle. The complex car model of 6 degrees of freedom is represented by a total of 16 state variables (Chen and Han Shue, 1998). We used the PATH car model (Figure 1) as a basis for our simulation. Because our main interest is with steering control, we ignored the roll, pitch and vertical movements of the vehicle. It is assumed that the vehicle runs on a flat road and that the lateral slip angle and the yaw angle are small (Huei and Masayoshi, 1990). The complex car model equation can be simplified if the speed of the vehicle is assumed to be constant. The curvature of the road was not considered in this study for simplifying the model, since the effect of the curvature on vehicle control at low speeds and large curvature radii is less than that of other uncertainties and external disturbances (Huei, 1992).

The linearized dynamic equation can be expressed as follows:

$$\frac{d}{dt}\begin{bmatrix} y_r \\ \dot{y}_r \\ \Psi_r \\ \dot{\Psi}_r \end{bmatrix} = \begin{bmatrix} 0 & 1 & 0 & 0 \\ 0 & \frac{A_1}{V} & -A_1 & \frac{A_2}{V} \\ 0 & 0 & 0 & 1 \\ 0 & \frac{A_3}{V} & -A_3 & \frac{A_4}{V} \end{bmatrix} \begin{bmatrix} y_r \\ \dot{y}_r \\ \Psi_r \\ \dot{\Psi}_r \end{bmatrix} + \begin{bmatrix} 0 \\ B_1 \\ 0 \\ B_2 \end{bmatrix} \delta_f , \tag{1}$$

where A_1, A_2, A_3, A_4, B_1 and B_2 are defined as

$$A_1 = -\frac{C_f + C_r}{m}, \qquad A_2 = -\frac{(C_f L_f - C_r L_r)}{m},$$

$$A_3 = \frac{(-C_f L_f + C_r L_r)}{J}, \qquad A_4 = -\frac{(C_f L_f^2 + C_r L_r^2)}{J},$$

$$B_1 = \frac{C_f}{m}, \qquad B_2 = \frac{C_f L_f}{J}.$$

The front wheel steering actuator is assumed to be dominated by the first-order delay.

$$\theta_m = \frac{1}{T_m s + 1} u_f , \tag{2}$$

where T_m is the time constant of the motor, u_f is the control input and θ_m is the motor (or steering wheel) angle.

The steering angle is limited to $|\delta_f| \le 22^\circ$. Also, the steering angle rate is limited to $|\dot{\delta}_f| \le 22^\circ/\text{s}$. The steering system from the motor (or steering wheel) angle θ_m to the wheel angle δ_f is modeled as a gear with gear ratio n. Therefor, δ_f is given by

$$\delta_f = n\,\theta_m . \tag{3}$$

Combining the dynamics of the actuator and the vehicle dynamics, a 5th order state space model with states $X=[y_r\ \dot{y}_r\ \Psi_r\ \dot{\Psi}_r\ \theta_m]^T$ is obtained as follows:

$$\dot{X}=\begin{bmatrix} 0 & 1 & 0 & 0 & 0 \\ 0 & \frac{A_1}{V} & -A_1 & \frac{A_2}{V} & B_1\cdot n \\ 0 & 0 & 0 & 1 & 0 \\ 0 & \frac{A_3}{V} & -A_3 & \frac{A_4}{V} & B_2\cdot n \\ 0 & 0 & 0 & 0 & -\frac{1}{T_m} \end{bmatrix} X+\begin{bmatrix} 0 \\ 0 \\ 0 \\ 0 \\ \frac{1}{T_m} \end{bmatrix} u_f . \tag{4}$$

The essential objective of this system is to drive the vehicle along the reference path by using the steering control device.

2.2. Lateral Control of Autonomous Vehicles

Figure 2 shows the H_∞ control block diagram. The components of w are all the exogenous inputs to the system (Kemin, 1998). These typically consist of disturbances, sensor noise reference commands and fictitious signals that drive frequency weights and models of the uncertainty in the dynamics of the system. The components of z are all the variables we wish to control, such as tracking errors and actuator signals. The inputs generated by the controller are denoted u. The sensor measurements used by the feedback controller are denoted y.

The generalized plant P, which is assumed to be linear and time-invariant, contains all the information that is favorable to incorporate into the synthesis of the controller, K. System dynamics, models of the uncertainty in the system's dynamics, frequency weights to influence the controller synthesis, actuator dynamics, sensor dynamics and implementation hardware dynamics are all included in P.

$$z=P_{11}w+P_{12}u \tag{5}$$
$$y=P_{21}w+P_{22}u \tag{6}$$
$$u=Ky \tag{7}$$

The relationship between the variable z and the exogenous input is $z=T_{zw}w$. The H_∞ control is represented as follows:

$$\|T_{zw}\|_\infty \le \gamma. \tag{8}$$

Equation (8) motivates the design of a stable controller of P to maintain a less infinite norm of T_{zw} than the given scalar γ.

The H_∞ control is represented as Equation (9) with the method of Glever and Doyle (John *et al.*, 1989).

$$\left\| \begin{matrix} W_1S \\ W_3S \end{matrix} \right\|_\infty \le \gamma. \tag{9}$$

In the mixed-sensitivity problem, W_1 and W_3 are

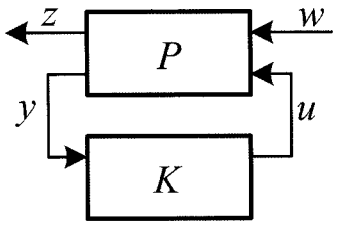

Figure 2. H_∞ controller block diagram.

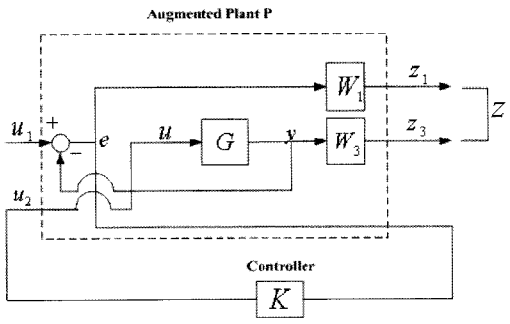

Figure 3. Standard feedback configuration of H_∞.

weighting functions for improving the performance of the system. In addition, S and T are the sensitivity function and the loop transfer function of the system, respectively. Figure 3 represents the construction of a H_∞ controller with a general weighting function as is used in the mixed-sensitivity problem.

The selection of weighting functions for a specific design problem often involves ad hoc fixing, many iterations and fine tuning. It is challnging to generate a general formula for weighting functions that applies to every case. Based on the time domain performance specifications, the corresponding requirements in a frequency domain in terms of the bandwidth ω_b and the peak sensitivity M_s can be determined. This assumes that the steady state error of the step response ε has to satisfy $|W_1(0)| \ge 1/\varepsilon$. A possible choice of W_1 can be obtained by modifying the weighting function as follows:

$$W_1=\frac{s/M_S+\omega_b}{s+\omega_b\varepsilon}. \tag{10}$$

W_1 is selected to improve the disturbance-reject and command-tracking, as follows:

$$W_1=\frac{0.1(s+500)}{(s+0.001)}. \tag{11}$$

Additionally, the magnitude of $|KS|$ in the low-frequency range is essentially limited by the allowable cost of control effort and saturation limit of the actuators; hence, in general, the maximum gain M_T of KS can be fairly large, while the high-frequency gain is essentially limited by the controller bandwidth (ω_{bc}) and the sensor

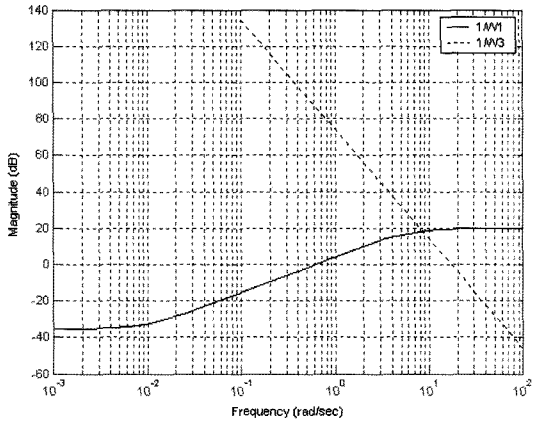

Figure 4. Selected weighting functions.

noise frequencies. A candidate weight W_3 would be

$$W_3=\frac{s+\omega_{bc}/M_T}{\varepsilon_1 s+\omega_{bc}} \tag{12}$$

for a small $\varepsilon_1 > 0$. Considering the roll off performance of the controller W_3 is selected to reject noise, as follows:

$$W_3=\frac{s^3}{2000}. \tag{13}$$

Figure 4 is the bode plot of each weighting function.

2.3. Simulation

The performance of the H_∞ controller as compared to the PID controller was evaluated by simulation. The reference input of the system was the reference yaw that was calculated by the current position and attitude of the vehicle and a target point. Furthermore, uncertainty parameters of the vehicle and noise were considered.

Figure 5 is the response of a system containing measurement noise. Figure 6, Figure 7 and Figure 8 are the responses for systems containing not only noise but also system uncertainty. System uncertainties also take into consideration the velocity and mass of the vehicle. Also considered are the noise factors of sensors when

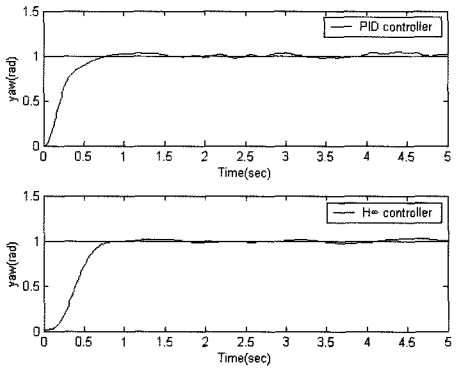

Figure 5. Simulation results (2.778 m/s, noise).

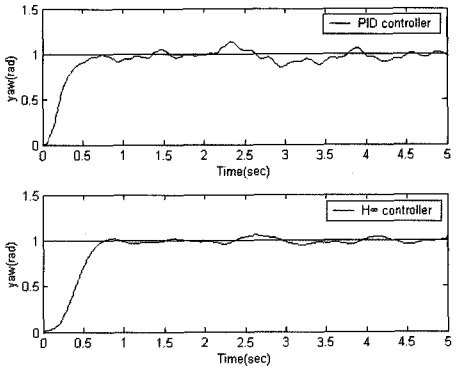

Figure 6. Simulation results (2.778 m/s, noise, +100 kg).

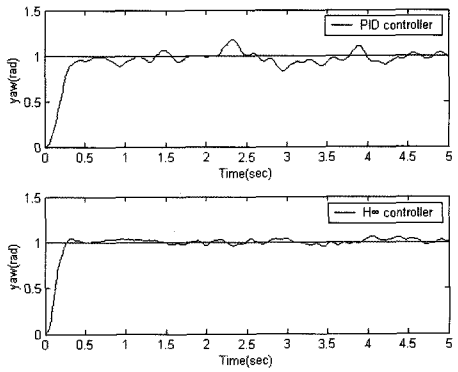

Figure 7. Simulation results (5.778 m/s, noise).

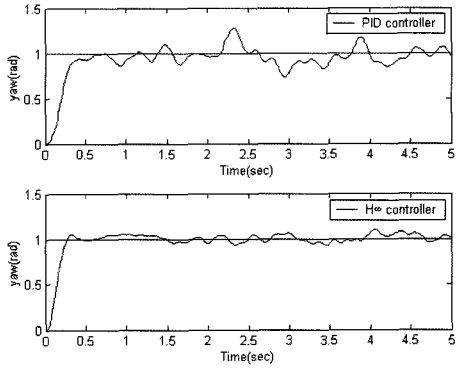

Figure 8. Simulation results (5.778 m/s, noise, +100 kg).

measuring position and attitude.

The result of the simulation showed that the H_∞ controller was more robust than the PID controller in the system.

3. NAVIGATION ALGORITHM

3.1. Concept of the Navigation Algorithm

Figure 9 shows the concept of the navigation algorithm that is introduced in this section. The navigation system acquires path data by using the RTK-DGPS. The path has

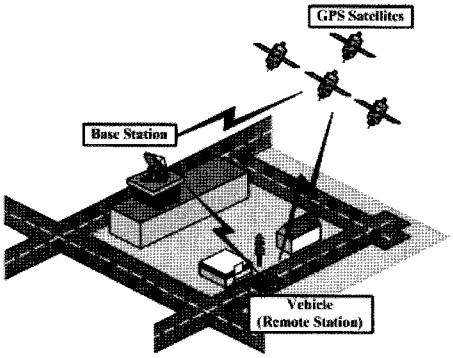

Figure 9. Integration concept of operation.

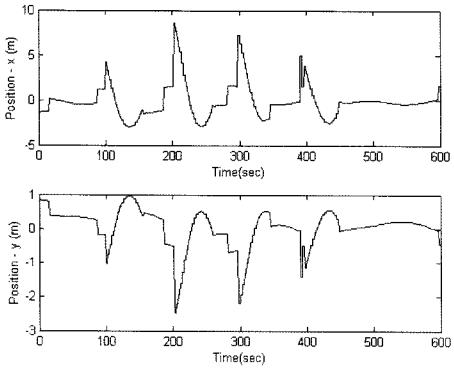

Figure 10. Fixed ECEF position without RTK-DGPS.

to reflect the curvature of the road. The path data is used to construct a virtual reference line and target points for navigation. The attitude of the vehicle is acquired by electric compass.

The RTK-DGPS has high position precision, because it uses carrier-phase measurements (Jay and Matthew, 1998). To obtain high accuracy with carrier-phase measurements, it is necessary to compute the number of GPS wavelengths between the roving GPS receiver and the satellites using the information from a base receiver. By this technique, the RTK-DGPS is accurate to the cm-level in dynamic environments.

Figure 10 and Figure 11 show differences of precision between GPS and RTK-DGPS. The variance of GPS x and y data is 8.579 m and 2.454 m, respectively. On the other hand, the variance of RTK-DGPS is 0.026 m and 0.021 m. The precision of the RTK-DGPS is therefore sufficient for navigation of real scale vehicles.

3.2. Navigation Algorithm

Figure 12 shows how target points are determined by using map data. The unmanned vehicle navigates the road by comparing its current position with map data. However, the navigation system cannot compare all data for searching target points. It therefore calculates the maximum moving distance r of the vehicle by using the

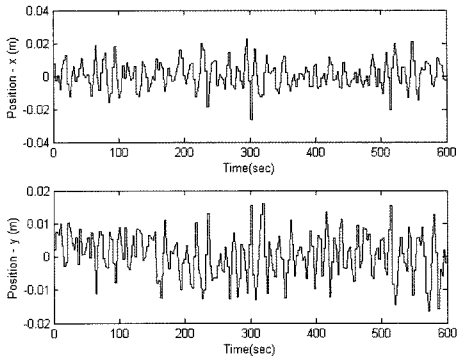

Figure 11. Fixed ECEF position with RTK-DGPS.

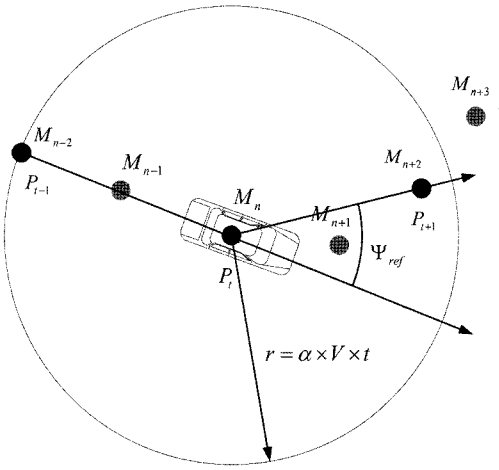

Figure 12. Navigation concept.

velocity of the vehicle until it acquires the next set of RTK-DGPS data. It compares the current position with the maximum distance position M_{n+2} within a circle with radius r. It calculates the yaw reference $|\psi_{ref}|$ by a vectors dot product. It uses the prior position P_{t-1}, the current position P_t and the target position M_{n+2}, which is shown in Equation (15) as follows:

$$|\psi_{ref}| = \cos^{-1} \frac{\overrightarrow{P_{t-1}P_t} \cdot \overrightarrow{P_tM_{t+2}}}{\left|\overrightarrow{P_{t-1}P_t}\right| \cdot \left|\overrightarrow{P_tM_{t+2}}\right|}. \tag{14}$$

The sign of direction is solved by using the sign of the vectors cross product, as follows:

$$\overrightarrow{P_{t-1}P_t} \times \overrightarrow{P_tM_{t+2}} = \begin{vmatrix} \vec{i} & \vec{j} & \vec{k} \\ P_{t-1}P_{t_x} & P_{t-1}P_{t_y} & P_{t-1}P_{t_z} \\ P_tM_{t+2_x} & P_tM_{t+2_y} & P_tM_{t+2_z} \end{vmatrix}. \tag{15}$$

We can acquire ψ_{ref} by using Equations (14) and (15):

$$\psi_{ref} = sign(\vec{k}(P_{t-1}P_{t_x} \times P_tM_{t+2_y} - P_{t-1}P_{t_y} \times P_tM_{t+2_x})) \times |\psi_{ref}|. \tag{16}$$

For determining the target point, r is calculated by

using the velocity V of the vehicle, sampling time (t) of the RTK-DGPS and α, the coefficient representing the curvature of the road. The coefficient α is used for determining the proper target point. If target points are calculated at 1 second intervals, the yaw variation severely increases. Therefore, angle data λ of the vectors are added to the path data by post-processing. The data are calculated using $n-1$th, n-th and $n+1$th data in the path data. The coefficient α is acquired by using Equation (17). The equation indicates that the far target point is selected in a straight course. Moreover, the target point considers the velocity of the vehicle as determined by the curvature of the road. The equation is optimized by simulation and experiments as follows:

$$\begin{cases} \lambda > 0.1rad, & \alpha=1 \\ \lambda > 0.1rad, & \alpha=180\lambda^2-37\lambda+3. \end{cases} \quad (17)$$

4. EXPERIMENT

4.1. Experimental System

Figure 13 shows the total composition of the system for the actual experiment. The experiment vehicle is the KIA SPORTAGE. The RTK-DGPS system is from the Z-family of Ashtech. The accuracy of the synchronized RTK mode is 0.5 cm+1 ppm. In addition, the maximum position output rate at the remote receiver is 1 Hz. The communication between the base station and the remote station in the vehicle was accomplished by using a PDL (Positioning Data Link) system that uses an RF connection. Additionally, we used a digital compass manufactured by Robot electronics. Its absolute error is 3°, with a resolution of 0.1°. Wheel sensors were used to measure vehicle velocity.

The GPS receiver and PDL rover were located on the roof of the vehicle and a motor driver, computer and power supply were installed in the trunk of the vehicle. Additionally, a digital compass was installed beneath the roof. Because the compass had to be isolated from magnetic fields caused by the rotation of spindles, a computer-controlled steering wheel mechanism was installed in the front seat of the vehicle. We installed the power transmission mechanism and gear to correspond to an exact control value. A PXI-1002 navigation computer (National Instrument) was used. Finally, the navigation software was coded by using LabVIEW 6.1.

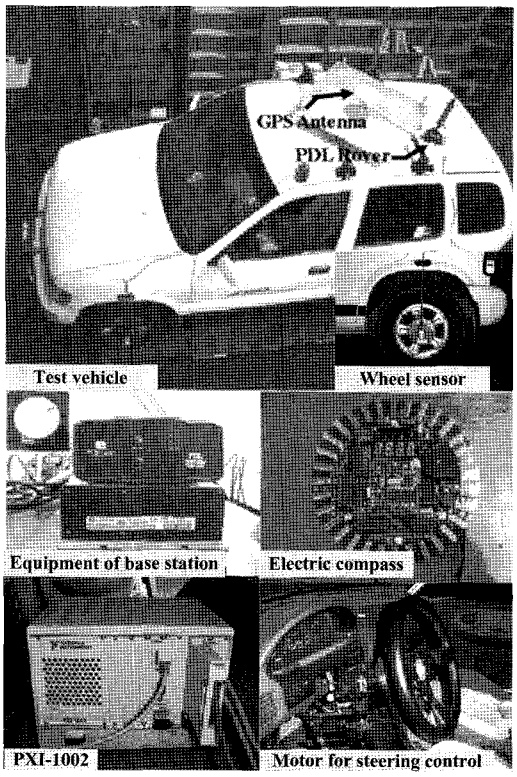

Figure 13. Total composition of the system.

4.2. Experiment Results

Figure 14 shows the area for the test. The base station was installed near this area. The width of the test road was a minimum of 3.6 m and the vehicle width was 1.735

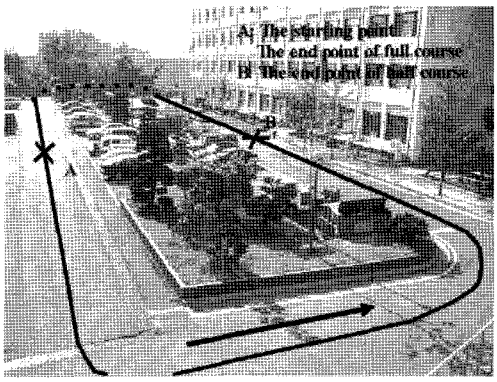

Figure 14. Photograph of test field.

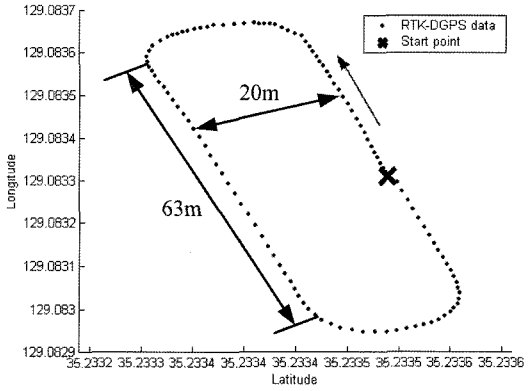

Figure 15. Acquired map data.

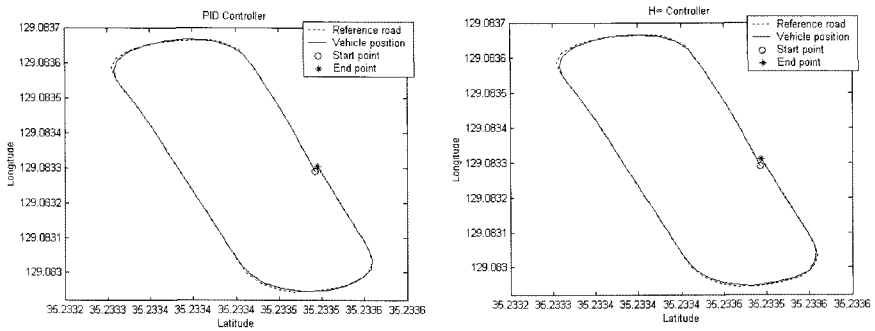

(a) PID controller (b) H_∞ controller

Figure 16. Trajectories for each lateral controller.

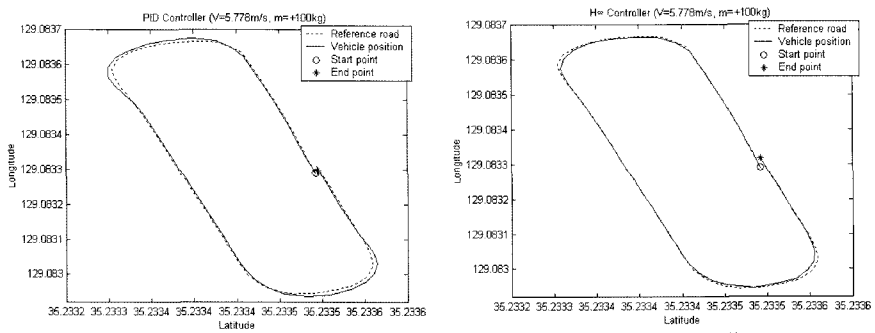

(a) PID controller (b) H_∞ controller

Figure 17. Trajectories for each lateral controller (+2 m/s, +100 kg).

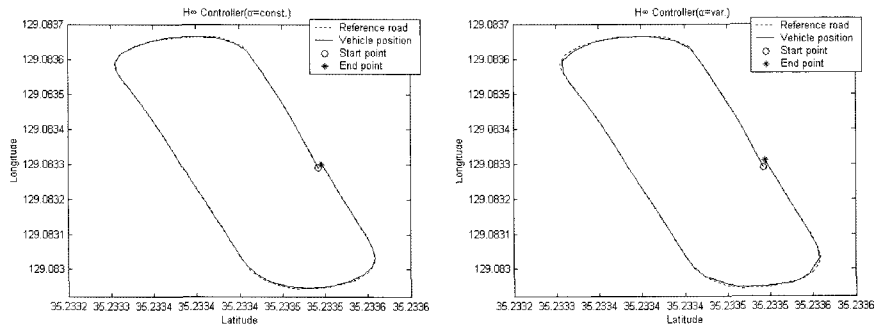

(a) α =constant (b) α =variable

Figure 18. Trajectories for considering change of yaw.

m. Before the test, the path data were acquired by using the RTK-DGPS. Figure 15 shows the path data. The distance of a full lap was 160 m.

The positions and attitudes of the vehicle at the start point of all experiment results were similar, but not identical. The differences are assumed to be negligible, as we are considering the overall tracking performance of the vehicle.

The velocity of the vehicle was about 2.778 m/s (about 10 km/h). Figure 16 shows the test results when the parameter is similar to that used in designing the controller. In Figure 17, the velocity and mass of the vehicle are changed in the test driving condition. This was done to compare performance of each controller while considering modeling uncertainty. The performance of the H_∞ controller is more robust than a PID controller for a change of system parameters. Figure 18 and Figure 19 show the performance of the coefficient α. The number of reference inputs is changed according to magnitude of changing road curvature. If α is a constant, the reference yaw angle is determined to within a small error. In the case of variable α, the number of yaw reference is decreased. As a result, more comfortable driving is possible. Table 1 presents the maximum and RMS of the

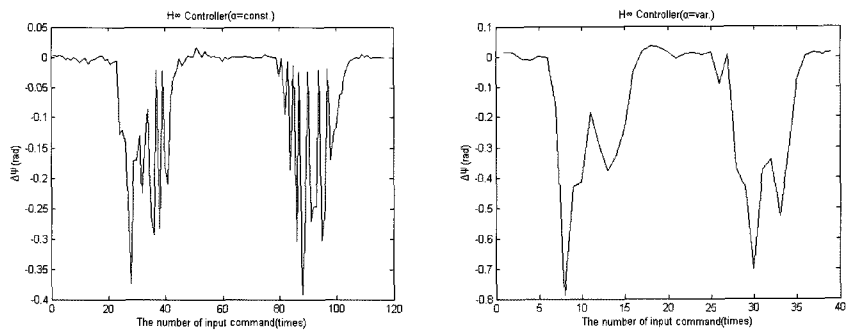

(a) α =constant (b) α =variable

Figure 19. The number of determining reference yaw angle.

Table 1. Results of driving test.

Test result	Maximum error [m]	RMS error [m]
PID	0.447	0.276
H_∞	0.521	0.220
PID(+2 m/s, +100 kg)	0.914	0.483
H_∞(+2 m/s, +100 kg)	0.732	0.310
H_∞(α=const., +100 kg)	0.431	0.264
H_∞(α=var., +100 kg)	0.402	0.282

errors of each experiment.

5. CONCLUSION

In this study, a vehicle model was used to verify the performance of a proposed lateral control and a simple navigation algorithm. An H_∞ control algorithm was applied to control the yaw of the vehicle.

To cope with sensor noise and modeling uncertainty, a robust lateral controller was designed to use the feedback of the yaw angle error of the vehicle. For position sensing of the vehicle, a reference lane was constructed by using the RTK-DGPS. The curvature of the road was considered in determining the target point from the map data. The reference map data were reconstructed to reduce the change in yaw of the vehicle. The position and attitude of the vehicle were calculated by using the RTK-DGPS and a digital compass. The vehicle was steered by an dc motor controlled by a real time module. The results from the vehicle model show that the proposed lateral controller improved the tracking performance. Although the autonomous vehicle was operated in a limited driving area at low speed, these results are applicable to a vehicle that is operated at a port, park or airport.

We also considered current related work concerned with improving the precision of dead reckoning by correction of the diameters of tires. In such cases, the vehicle navigates for a longer time by dead reckoning in an urban canyon environment. We expect such applications will be useful in the future to create a wheelchair system for blind.

ACKNOWLEDGEMENT–This work was supported by the second stage of the Brain Korea 21 Project.

REFERENCES

Broggi, A., Bertozzi, M. and Fascioli, A. (1999). ARGO and the millemiglia in autoatico tour. *IEEE Intelligent System* **14**, **1**, 55–64.

Chen, C. and Han Shue, T. (1998). Steering control of gigh speed vehicles: Dynamic look ahead and yaw rate feedback. *Proc. 37th IEEE Conf. and Decision & Control*, 1025–1030.

Chen, C., Guldner, J., Kanellakopoulous, I. and Tomizuke, M. (1998). Nonlinear damping in vehicle lateral control: Theory and experiment. *Proc. American Control Conf.*, 2243–2247.

Huei, P. (1992). *Vehicle Lateral Control for Highway Automation*. Ph. D. Dissertation. University of California. Berkeley.

Huei, P. and Masayoshi, T. (1990). *Lateral Control of Front-Wheel-Steering Rubber-Tire Vehicles*. UCB-ITS-PRR-90-5. PATH Research Report. California.

Huei, P., Wei-Bin, Z., Alan, A., Ye, L., Thomas, H., Peter, D., Masayoshi, T. and Steven, S. (1992). *Experimental Automatic Lateral Control System for an Automobile*. PATH Research Report. California

Jay, F. and Matthew, B. (1998). *The Global Positioning System and Inertial Navigation*. 1st edn.. McGraw-Hill. New York.

John, C., Keith, G, Pramod, P. and Bruce, A. (1989). State-space solutions to standard H_2 and H_∞ control problems. *IEEE Trans. Automatic Control* **34**, **8**, 831–847.

Kemin, Z. (1998). *Essential of Robust Control*. 1st edn.. Prentice-Hall. New Jersey.

Lee, D. E., Yoo, S. H. and Kim, Y. B. (2006). Stable

autonomous driving method using modified OTSU algorithm. *Int. J. Automotive Technology* **7**, **2**, 227–235.

Lee, K. B., Kim, Y. J., Ahn, O. S. and Kim, Y. B. (2002). Lateral control of autonomous vehicle using levenberg-marquardt neural network algorithm. *Int. J. Automotive Technology* **3**, **2**, 71–77.

Miguel Angel, S., Sergio, A., Jesus, R., Eugenio Garcia, J., Teresa, P. and Carlos, G. (2001). Vehicle fuzzy driving based on DGPS and vision. *Proc. IFSA World Congress and 20th NAFIPS Int. Conf.*, **3**, 1472–1477.

Naranjo, J. E., Gonzalez, C., Garcia, R., Pedro, T. and Haber, R. (2005). Power-steering control architecture for autonomous driving. *IEEE Trans. Intelligent Transportation System* **6**, **4**, 406–415.

Ryu, J. H., Chang, Y. S., Park, G. H., Lee, C. H., Park, S. H. and Lee, M. H. (2004). Research on navigation system of an autonomous vehicle using RTK-DGPS. *Proc. 30th Annual Conf. IEEE Industrial Electronics Society*, **2**, 1716–1720.

Shladover, S. (1991). Automated vehicle control developments in the PATH program. *IEEE Trans. Vehicular Technology* **40**, **1**, 114–130.

Tan, H. S., Farrell, J. A. and Yang, Y. (2003). Automatic vehicle steering controls: DGPS/INS and magnetic markers. *Proc. American Control Conf.*, **1**, 60–65.